Acta Acustica united with Acustica
Vol. 97 (2011) 966 – 973

DOI 10.3813/AAA.918478

Fast Computation of the Scattering Matrix of Lined Ducts Containing Passive Components

Romain Maréchal[1)], Emmanuel Perrey-Debain[1)], Jean-Michel Ville[1)], Benoit Nennig[2)]

[1)] Université Technologique de Compiègne, Laboratoire Roberval UMR CNRS 6253, BP 20529, 60205 Compiègne Cédex, France. emmanuel.perrey-debain@utc.fr

[2)] Laboratoire d'Acoustique de l'Université du Maine UMR CNRS 6613, Avenue Olivier Messiaen, 72085 Le Mans Cédex 9, France

Summary

This paper deals with strategies for computing efficiently the propagation of sound waves in lined ducts containing passive components. In most cases of practical interest, these added acoustics components can be modelled as acoustic cavities which are connected to the duct and can be either purely reactive or dissipative. The assessment of the efficiency of such a system requires a precise knowledge of the acoustic field in the duct. In the present work a new numerical procedure that judiciously exploit the benefit of the FEM and the mode matching approach is presented. First, a set of FE eigenmode are computed in the cavity to produce a numerical impedance matrix connecting the pressure and the acoustic velocity on the duct wall interface. Then an integral representation for the acoustic pressure in the main duct is used. The presence of acoustic liners on the walls of the duct is taken into account via an appropriate modal decomposition of the Green's function. Typical applications involving Helmholtz resonators and side branch ducts (Herschel-Quincke tubes) are presented. We show that our algorithm allows a very fast and accurate computation of the scattering matrix of such a system with a numerical complexity that grows very mildly with the frequency.

PACS no. 43.20.Mv, 43.50.Gf, 43.55.Ka

1. Introduction

In a large number of sound generating devices, sound waves of large amplitude are being set up inside a tube and some of the acoustic energy propagate in the duct before being radiated into the open. The practical applications of such systems range from noise transmission in vehicle exhaust systems, through ventilation and air conditioning ducts, to sound propagation in the ducted regions of turbofan aircraft engines.

The acoustic energy flow reduction techniques for the duct noise problem can be divided into two categories. Reactive techniques specifically aim to alter the duct impedance by reflecting back most of the incident acoustic wave. In most cases of practical interest, these acoustics components can be modeled as acoustic cavities which are connected to the duct. Dissipative techniques specifically aim to absorb the sound field as it propagates down the duct. These most commonly take the form of a lining material (porous and/or perforate metal panel) placed on the walls of the duct. While these absorbent materials are known to be typically effective at relatively high frequencies and for broadband attenuation, reactive techniques, usually best applied to low frequency noise problems, offers more localized attenuation in the frequency domain. For these reasons, these techniques seem to have reached their limit when used on their own and there is still a need to consider the benefit of these two combined in order to reduce further the sound radiation at the duct exit, see for instance [1, 2].

The assessment of the efficiency of such a system requires a precise knowledge of the acoustic field in the duct. Though standard Finite Element (FE) software could, in principle, be used for this purpose, a full FE model would be extremely demanding as the number of variables is expected to grow like f^d (f is the frequency and $d = 2, 3$ the dimension of the discretized domain). To make the matter worse, the FE method is known to suffer from pollution errors which can be avoided at a price of a very high discretization level especially in the medium and high frequency range [3, 4]. In fact, most researchers seem to favor the use of the Boundary Element method (BEM) for their numerical prediction [3, 5, 6, 7]. The BEM has the great advantage that only the boundary of the acoustic domain needs to be discretized. However, the method is still limited to 'low frequency' applications as the number of unknowns must not exceed few thousands on a personal computer. All this makes standard methods (FEM and BEM) cumbersome and time-consuming both in terms of data preparation and computation. This can have a neg-

Received 7 June 2011,
accepted 9 August 2011.

ative impact when some efficient optimizations regarding the geometry and position of these added components for instance are needed.

In this paper, we are dealing specifically with acoustic ducts comprising (i) a finite length of acoustic liner at its wall where it is assumed that the surface is locally reacting and (ii) the presence of passive components connected to the lined section of the duct. We present a new numerical procedure that judiciously exploit the benefit of the FEM and the mode matching approach for the fast computation of the scattering matrix for such a system. The idea relies mainly on the concept of impedance matrix that connects the pressure to the acoustic normal velocity on the duct-cavity interface. This considerably reduces the number of variables as only the interface needs to be discretized. The description of the acoustic pressure in the lined section of the main duct is carried out using integral equations with appropriate modal decomposition of the Green's function. The theory is presented in sections 3 and 4. The last section shows practical applications involving Helmholtz resonators [5] and Herschel-Quincke tubes [8]. The benefit of the present approach is shown both in term of CPU time and model reduction, when compared to standard FEM models.

2. Problem statement

The problem under consideration is illustrated in Figure 1. It consists of a two-dimensional lined main duct (domain Ω) of height h which is connected to a single cavity Ω_c. The inlet and outlet pipes (regions I and II) are identical, each having rigid walls at its boundaries Γ_w. We wish to evaluate the scattering matrix (or S-matrix) of this acoustic system, that is given incident pressure waves P_{I}^+ and P_{II}^-, we compute the scattered waves P_{I}^- and P_{II}^+. We call Γ_1 (resp. Γ_2) the lined wall of the main duct with impedance Z_1 (resp. Z_2).

In the main duct and in the cavity the acoustic pressure p satisfies the Helmholtz equation

$$\Delta p + k^2 p = 0. \tag{1}$$

On the lined walls Γ_1 and Γ_2 , a local impedance condition is prescribed,

$$Z_e = \frac{1}{Y_e} = \frac{p}{\mathbf{v}\cdot\mathbf{n}}, \quad e = 1, 2. \tag{2}$$

Note the impedance Z_e (or the admittance Y_e) is generally function of the frequency and the acoustic normal velocity is proportional to the pressure gradient, i.e. $\partial_n p = \mathrm{i}\omega\rho\mathbf{v}\cdot\mathbf{n}$ where $\mathbf{n}$ is the outward unit normal. Here, we adopt the $\mathrm{e}^{-\mathrm{i}\omega t}$ -convention, $k = \omega/c$ is the wave number, c the celerity, ω the angular frequency, ρ the fluid density. The transmission conditions at the artificial boundaries Γ_{I} and Γ_{II} are given from the pressure wave field in the inlet and outlet pipes. This is expressed as the usual modal series

$$P_l^{\pm} = \sum_{m=0}^{\infty} A_{l,m}^{\pm} \psi_m^0(x) \mathrm{e}^{\pm \mathrm{i}\beta_m^0 z}, \tag{3}$$

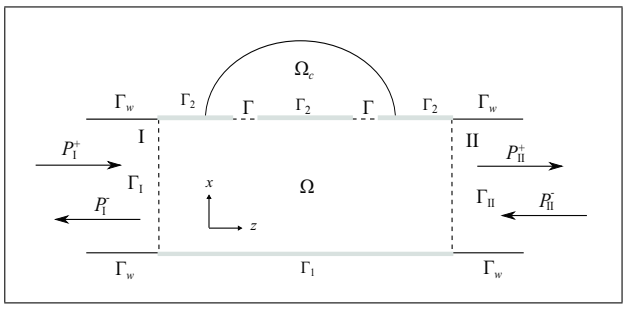

Figure 1. Main duct with a single passive component.

where l = I or II. Here the pair (ψ_m^0, β_m^0) defines the classical propagative or evanescent mode in the rigid pipe and the superscript 0 refers to the rigid wall case. Finally, we require that p and its normal derivative (i.e. the normal velocity) to be continuous across the duct-cavity interface Γ.

3. Impedance matrix: general theory for purely reactive components

In this section we shall present the general procedure for constructing impedance matrices associated with a cavity filled with air with rigid walls. We first assume that the acoustic cavity Ω_c is closed, that is we enforce Neumann rigid boundary conditions on the apertures Γ. Standard results show there exists a complete set of orthogonal eigenfunction Φ_n belonging to the spectrum of the Laplacian operator [9],

$$\Delta\Phi_n = -k_n^2\Phi_n, \tag{4}$$

subject to the boundary conditions: $\partial_n\Phi_n = 0$. Now, any given pressure field in Ω_c can be written as a weighted sum of the eigenfunctions. In particular, the Green's function for the cavity, which satisfies

$$\Delta G_c + k^2 G_c = -\delta(\boldsymbol{x} - \boldsymbol{x}_0), \tag{5}$$

is given by the infinite series

$$G_c(\boldsymbol{x}, \boldsymbol{x}_0, \omega) = \sum_{n=0}^{\infty} \frac{\Phi_n(\boldsymbol{x})\Phi_n(\boldsymbol{x}_0)}{\omega^2 - \omega_n^2}, \tag{6}$$

where for the sake of clarity, we put $\omega_n = k_n c$. Eigenfunctions are properly normalized so that application of the Green's theorem in the cavity yields

$$p(\boldsymbol{x}) = \int_\Gamma G_c\, \partial_n p\, \mathrm{d}\gamma(\boldsymbol{x}_0), \tag{7}$$

where we omitted the $\boldsymbol{x}$ and $\boldsymbol{x}_0$ dependence in the integrand for the sake of clarity. The integral equation (7) is a classical result which is the starting point for the BEM [10]. A specific feature of the present formulation is that the integration is limited to the duct-cavity interface and that the equation remains valid when the evaluation point is taken on the boundary Γ. Applying standard collocation

techniques to (7) and using linear interpolation for the normal velocity leads to the linear system,

$$\mathbf{p}_{\text{int}} = \mathbf{Z}(\omega)\,\tilde{\mathbf{F}}\,\partial_n \mathbf{p}_{\text{int}}. \tag{8}$$

Here, the vector $\mathbf{p}_{\text{int}}$ (resp. $\partial_n \mathbf{p}_{\text{int}}$) contains the discrete nodal values of the pressure (resp. normal derivative pressure) on the interface and, in this context, the frequency-dependent matrix $\mathbf{Z}$ can be interpreted as an impedance matrix. The matrix $\tilde{\mathbf{F}}$ stems from discretization of the boundary integral, its exact form is not essential for the moment as this will be clarified later. Without loss of generality, it is easy to see from (6), that this matrix admits the following truncated eigenmode decomposition

$$\mathbf{Z}(\omega) = \tilde{\mathbf{\Phi}}\,\mathbf{D}(\omega)\,\tilde{\mathbf{\Phi}}^{\mathrm{T}} + \mathbf{R}(\omega). \tag{9}$$

The matrix $\tilde{\mathbf{\Phi}} = (\tilde{\mathbf{\Phi}}_1 \cdots \tilde{\mathbf{\Phi}}_N)$ contains in its columns the nodal value of the eigenfunctions Φ_n $(n = 0, 1, \ldots, N)$ and $\mathbf{D}$ stands for the diagonal matrix with entries,

$$(\mathbf{D})_{nn} = (\omega_n^2 - \omega^2)^{-1}. \tag{10}$$

Here the tilde symbol means that we only retain the nodal values of these eigenmodes on the duct-cavity interface Γ. The interest for the decomposition (9) becomes clearer when the frequency of interest is taken well below the highest modal 'resonant' frequency (i.e. $|\omega - \omega_N|^{-1} \ll 1$). In this frequency range, the correction term $\mathbf{R}$ (also known as the static correction) is weakly dependent on the frequency, so we can take the low order Taylor expansion

$$\mathbf{R}(\omega) \approx \mathbf{R}(\overline{\omega}) + (\omega - \overline{\omega})\frac{\partial \mathbf{R}}{\partial \omega}(\overline{\omega}) + \ldots, \tag{11}$$

where $\overline{\omega}$ is a reference value to be specified later. Once the matrix $\mathbf{R}(\overline{\omega})$ and its derivatives have been stored, the computation of (9) becomes a very fast and simple procedure. Its efficiency relies on the numerical computation of a sufficiently large set of eigenfunctions as well as finding the residual matrix. In this work, a finite element strategy is used to discretize the exact geometry of the cavity so that no assumption is made a priori regarding the shape of the acoustic eigenmodes. We consider a finite element mesh made of two-dimensional linear triangular elements and we denote by ϕ_i the associated piecewise linear shape function. For the sake of illustration, a typical mesh corresponding to the discretization of a Helmholtz resonator with extended neck is shown in Figure 2. Cavity modes are also shown in the next section (see Figure 4).

Standard procedure leads to the following algebraic eigenmode problem:

$$\mathbf{A}(\lambda_n)\mathbf{\Phi}_n = 0 \quad \text{with} \quad \mathbf{A}(\lambda) = \mathbf{K} - \lambda \mathbf{M}, \tag{12}$$

where we put $\lambda = \omega^2$ for convenience, mass and stiffness matrices are given by

$$(\mathbf{M})_{ij} = \frac{1}{c^2}\int_{\Omega_c} \phi_i \phi_j \,\mathrm{d}\Omega$$

$$\text{and} \quad (\mathbf{K})_{ij} = \int_{\Omega_c} \nabla\phi_i \nabla\phi_j \,\mathrm{d}\Omega. \tag{13}$$

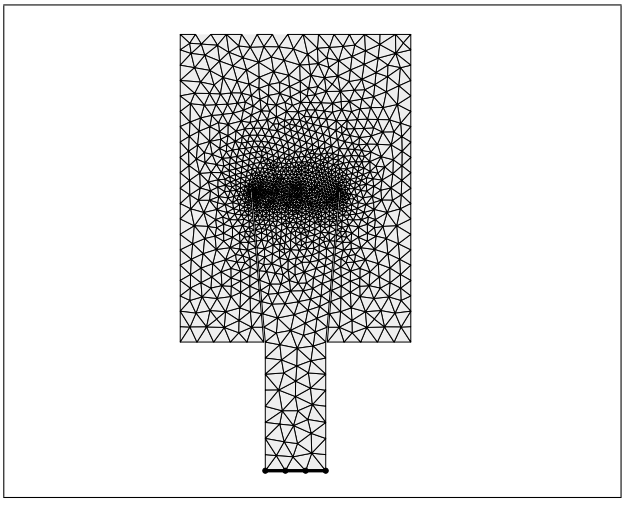

Figure 2. Typical triangular mesh for the Helmholtz resonator. The cavity-duct interface is in bold and FE nodes are identified by a black circle.

Equation (12) constitutes a generalized eigenvalue problem. Depending on the matrix size (i.e. the number of FE nodes in the whole cavity) and the number of modes retained in the series, the evaluation of the impedance matrix might be computationally expensive as this needs to be done for each frequency. This point will be discussed at the end of the section. A first set of N modes $(n = 0, 1, \ldots, N)$ is then computed using appropriate large sparse eigenvalue problem solvers where it is understood that the truncation order N is taken well below the FE matrix size. Now, finding the residual matrix is a bit more tricky as we first need to go back to the original direct problem,

$$\mathbf{A}(\lambda)\mathbf{p} = \mathbf{F}\,\partial_n \mathbf{p}_{\text{int}}, \tag{14}$$

where the vector $\mathbf{p}$ contains the value of the pressure at all nodes of the FE mesh. To ease the demonstration, we proceed to an appropriate elements reordering so that the rectangular matrix $\mathbf{F}$ looks like

$$\mathbf{F} = \begin{pmatrix} \tilde{\mathbf{F}} \\ \mathbf{0} \end{pmatrix} = \mathbf{I}_\Gamma \tilde{\mathbf{F}} \quad \text{with} \quad (\tilde{\mathbf{F}})_{ij} = \int_\Gamma \phi_i \phi_j \,\mathrm{d}\gamma. \tag{15}$$

Here $\mathbf{I}_\Gamma$ denotes the identity matrix for nodes on the interface only. Inverting (14) shows that the impedance matrix has the alternative form

$$\mathbf{Z}(\lambda) = \mathbf{I}_\Gamma^{\mathrm{T}}\,\mathbf{A}^{-1}(\lambda)\,\mathbf{I}_\Gamma. \tag{16}$$

The residual matrix is then computed simply via

$$\mathbf{R} = \mathbf{Z} - \tilde{\mathbf{\Phi}}\,\mathbf{D}\,\tilde{\mathbf{\Phi}}^{\mathrm{T}}, \tag{17}$$

and the first order derivative can be computed from

$$\frac{\partial \mathbf{R}}{\partial \lambda} = \mathbf{I}_\Gamma^{\mathrm{T}}\,\mathbf{A}^{-1}\mathbf{M}\,\mathbf{A}^{-1}\mathbf{I}_\Gamma - \tilde{\mathbf{\Phi}}\,\frac{\partial \mathbf{D}}{\partial \lambda}\,\tilde{\mathbf{\Phi}}^{\mathrm{T}}. \tag{18}$$

Note that (i) the ω-derivative is recovered from $\partial_\lambda \mathbf{R} = 2\omega\partial_\omega \mathbf{R}$ and (ii) the λ-derivative of the diagonal matrix $\mathbf{D}$

is an easy task as eigenvalues $\lambda_n = \omega_n^2$ are frequency-independent in the rigid wall case. Now exploiting the symmetry of $\mathbf{A}$, we see that $\mathbf{I}_\Gamma^{\mathrm{T}}\mathbf{A}^{-1} = (\mathbf{A}^{-1}\mathbf{I}_\Gamma)^{\mathrm{T}}$. Thus the important point to make is that the full inversion of $\mathbf{A}$ is not needed here. Only the first columns of $\mathbf{A}^{-1}$ corresponding to the interface nodes are active and these can be efficiently computed by solving successively $\mathbf{A}\mathbf{v}_i = \mathbf{e}_i$ with appropriate sparse solvers ($\mathbf{e}_i$ is the column vector with zero elements with the unity on the ith line). It is clear that the reference value $\overline{\lambda}$ must be chosen away from the resonant value λ_n to guarantee that the inversion of $\mathbf{A}$ is not spoiled by round off errors. In this work we take $\overline{\lambda} = \lambda_1/2$ and the value $\overline{\lambda} = \lambda_0 = 0$ is proscribed here as it corresponds to the rigid motion resonance. The formulation (7) is instructive, if for instance lossy walls with complex-valued impedance are present in the cavity. In this case the integral formulation remains valid [9] except eigenvalues and eigenmodes are now frequency-dependent, i.e. $k_n = k_n(\omega)$. This scenario is not considered in this work but this could be subject of further investigation by the authors.

4. S-matrix of the acoustic system

In the main duct, the theory starts by introducing the lined-walled duct Green's function satisfying the usual modal radiation condition on both ends of the main duct [9], i.e.

$$G(\boldsymbol{x}, \boldsymbol{x}_0) = \sum_{n=0}^{\infty} \frac{\psi_n(x)\psi_n(x_0)}{-2\mathrm{i}\beta_n} \mathrm{e}^{\mathrm{i}\beta_n|z-z_0|}, \tag{19}$$

where $\boldsymbol{x} = (x, z)$ and $\boldsymbol{x}_0 = (x_0, z_0)$ are two points in the domain Ω. Function ψ_n is the transverse mode, i.e.

$$\psi_n'' + \alpha_n^2\psi_n = 0 \tag{20}$$

and satisfying the lined-wall conditions (2) on both sides $x = 0$ and $x = h$ (here the prime signifies derivation with respect to the transverse coordinate x). By construction, transverse mode are orthogonal in the following sense

$$\int_0^h \psi_m(x)\psi_n(x)\,\mathrm{d}x = \delta_{n,m}. \tag{21}$$

Because ψ_n is complex-valued, (21) does not define a scalar product, i.e. functions are not complex conjugate, and there exist situations for which modes can not be normalized. It can be shown that this occurs for some discrete values for the impedance wall. The interested reader can refer to a recent paper [11] for more details. Fortunately these are 'pathological' scenarios which are extremely unlikely to happen and there is no need to comment further on this.

Solutions of (20) are of the form $\psi = A\cos(\alpha x) + B\sin(\alpha x)$ where transverse 'resonant' wavenumbers are found so that the 2×2 system

$$\begin{pmatrix} \mathrm{i}\rho\omega Y_1 & \alpha \\ \mathrm{i}\rho\omega Y_2\cos(\alpha h)+\alpha\sin(\alpha h) & \mathrm{i}\rho\omega Y_2\sin(\alpha h)-\alpha\cos(\alpha h) \end{pmatrix} \cdot \begin{pmatrix} A \\ B \end{pmatrix} = \begin{pmatrix} 0 \\ 0 \end{pmatrix} \tag{22}$$

admits non trivial solutions. After introducing the new parameter $\epsilon = \mathrm{i}\rho\omega Y_1 h$, the transverse wavenumbers are the roots of the dispersion equation

$$f(\tilde{\alpha}) = -\tilde{\alpha}^2\sin\tilde{\alpha} - (1+\chi)\epsilon\tilde{\alpha}\cos\tilde{\alpha} + \chi\epsilon^2\sin\tilde{\alpha} = 0, \tag{23}$$

where $\tilde{\alpha} = \alpha h$ and the dimensionless quantity χ stands for the impedance ratio: $\chi = Y_2/Y_1$. (Note in the limiting case where $Y_1 \to 0$ whereas Y_2 remains fixed it is more judicious to swap Y_2 with Y_1 in the dispersion equation). Because function f is an odd function, it suffices to consider values in the half-plane : $\Re(\alpha) \geq 0$. For sufficiently small ϵ, it is natural to seek asymptotic solutions as the truncated power series [9]

$$\tilde{\alpha}_n = \alpha_n h = n\pi + \sum_{l=1}^{K} a_{l,n}\epsilon^l, \tag{24}$$

so that when $\epsilon = 0$, rigid wall modes are recovered. After substituting (24) in (23) and equating coefficients of like powers (in ϵ) yield a hierarchy of equations for expansion coefficients $a_{l,n}$. This operation can be easily carried out using symbolic computation softwares (we choose MAPLE here). For completeness sake, the expression for the first four coefficients are

$$\begin{aligned} a_{1,n} &= -\frac{1+\chi}{n\pi}, \qquad a_{2,n} = -\frac{(1+\chi)^2}{(n\pi)^3}, \\ a_{3,n} &= \frac{1+\chi^3}{3(n\pi)^3} - \frac{2(1+\chi)^3}{(n\pi)^5} \\ \text{and} \quad a_{4,n} &= \frac{4(1+\chi)(1+\chi^3)}{3(n\pi)^5} - \frac{5(1+\chi)^4}{(n\pi)^7}. \end{aligned} \tag{25}$$

Obviously, the asymptotic approach can not be used for the fundamental mode ($n = 0$) and is slowly converging, or even not converging at all, for the lowest-order modes especially as the frequency increases. For these latter, root finding algorithms must be employed. In this context, the Newton-Raphson method is probably the most reliable technique as long as good initial guesses are available. In the present work, initial guesses are found from the low frequency limit $\omega = \epsilon = 0$ corresponding to the rigid wall solutions. The frequency is then incremented upwards with a sufficient small frequency step to ensure that roots found at starting frequency can be used as the initial guesses for the following frequency. It was observed however that the fundamental mode might show a singular behavior in the limit $\epsilon \to 0$ and thus deserves a special treatment. Here we used a technique described by Kravanja [12] and already used by the some of the authors for the modeling of dissipative silencers [13]. The method exploits the fact $f(\tilde{\alpha})$ is analytic in the complex $\tilde{\alpha}$-plane allowing to solve (23) using Argument Principle. Although the procedure is relatively more time consuming, it is done only once for a specific starting frequency. Another alternative used in [11] is to compute approximate initial guesses for low order modes of (21) using standard

discretization schemes on a coarse mesh. Once transverse wavenumbers have been found, modes are given from

$$\psi_n(x) = N_n \left(\cos(\alpha_n x) - \mathrm{i}\rho\omega Y_1 \frac{\sin(\alpha_n x)}{\alpha_n} \right), \quad (26)$$

and normalisation coefficients N_n are obtained from (21) (note this operation is inexpensive as these quantities are computed analytically). Finally, axial wavenumbers in (19) are computed by inverting the dispersion equation:

$$\beta_n = \sqrt{k^2 - \alpha_n^2} \quad (27)$$

with the convention that $\Im(\beta_n) \geq 0$ so it corresponds to right-propagating waves.

Now, using the Green's theorem, the pressure anywhere in the lined section of the duct is given via the integral representation

$$p(\boldsymbol{x}) = \int_{\Gamma_\mathrm{I} \cup \Gamma_\mathrm{II}} (G\, \partial_n p - p\, \partial_n G)\ \mathrm{d}\gamma(\boldsymbol{x}_0) + \int_\Gamma G\, (\partial_n p - \mathrm{i}\rho\omega Y_2 p)\ \mathrm{d}\gamma(\boldsymbol{x}_0), \quad (28)$$

where we used the fact that $\partial_n G = \mathrm{i}\rho\omega Y_2 G$ at $x = h$. The discretization of this equation is carried out in two steps. First, collocating (28) at the FEM nodes of the duct-cavity interface leads to

$$\mathbf{K}_{\Gamma,\Gamma}\, \partial_n \mathbf{p}_\mathrm{int} + \mathbf{K}_{\Gamma,\mathrm{I}}\, \mathbf{A}_\mathrm{I}^- + \mathbf{K}_{\Gamma,\mathrm{II}}\, \mathbf{A}_\mathrm{II}^+ = \mathbf{F}_{\Gamma,\mathrm{I}}\, \mathbf{A}_\mathrm{I}^+ + \mathbf{F}_{\Gamma,\mathrm{II}}\, \mathbf{A}_\mathrm{II}^-, \quad (29)$$

where vectors $\mathbf{A}_l^\pm$ contain the modes amplitudes $A_{l,m}^\pm$, (l=I,II). The first block matrix

$$\mathbf{K}_{\Gamma,\Gamma} = -\mathbf{Z}(\omega)\, \tilde{\mathbf{F}} - \mathbf{G} - \mathrm{i}\rho\omega Y_2 \mathbf{G}\mathbf{Z}(\omega)\, \tilde{\mathbf{F}} \quad (30)$$

stems from the self interaction of the acoustic pressure at the interface and we used the impedance relationship (8). Here the Green matrix $\mathbf{G}$ stems from the discretization of the second integral in (28). To fix the ideas, we consider that the cavity is connected on the upper side of the duct and we let $\boldsymbol{x}_i = (h, z_i)$ be a node located on the interface. Typical integrals over a linear element belonging to the interface Γ, i.e. with the parametrization: $\boldsymbol{x}_0(\eta) = (h, a + \eta b)$ and $\eta \in [-1, 1]$, involved in the computation of the Green matrix have the general form

$$\int_{-1}^{1} G(\boldsymbol{x}_i, \boldsymbol{x}_0(\eta))(1 \pm \eta)\ \mathrm{d}\eta = \sum_{n=0}^{\infty} \frac{\psi_n^2(h)}{-2\mathrm{i}\beta_n} \int_{-1}^{1} (1 \pm \eta)\, \mathrm{e}^{\mathrm{i}\beta_n |a+\eta b - z_i|}\ \mathrm{d}\eta. \quad (31)$$

Since the node $\boldsymbol{x}_i$ is either on the right or the left of the element, the quantity in the absolute value does not change sign in the integration interval and these integrals can be computed analytically independently of the node location. This fact is used in our algorithm to speed up the computation.

Other matrices are built by substituting $p = P_l^+ + P_l^-$ and $\partial_n p = \partial_n (P_l^+ + P_l^-)$ with (l=I,II) in the first integral of (28). This operation requires the computation of the coupling coefficients C_{mn} given by the overlap integrals

$$C_{mn} = \int_0^h \psi_m^0(x) \psi_n(x)\ \mathrm{d}x, \quad (32)$$

which also arise in standard mode matching techniques. The system (29) is completed by taking the evaluation point in the integral equation on the inlet and outlet boundaries. An additional set of equations is then produced by projecting (28) onto the hard-wall modes basis to give

$$\mathbf{K}_{l,\Gamma}\, \partial_n \mathbf{p}_\mathrm{int} + \mathbf{K}_{l,\mathrm{I}}\, \mathbf{A}_\mathrm{I}^- + \mathbf{K}_{l,\mathrm{II}}\, \mathbf{A}_\mathrm{II}^+ = \mathbf{F}_{l,\mathrm{I}}\, \mathbf{A}_\mathrm{I}^+ + \mathbf{F}_{l,\mathrm{II}}\, \mathbf{A}_\mathrm{II}^- \quad (33)$$

for both boundaries l = I and II. Now, by calling

$$\mathbf{K} = \begin{pmatrix} \mathbf{K}_{\Gamma,\Gamma} & \mathbf{K}_{\Gamma,\mathrm{I}} & \mathbf{K}_{\Gamma,\mathrm{II}} \\ \mathbf{K}_{\mathrm{I},\Gamma} & \mathbf{K}_{\mathrm{I},\mathrm{I}} & \mathbf{K}_{\mathrm{I},\mathrm{II}} \\ \mathbf{K}_{\mathrm{II},\Gamma} & \mathbf{K}_{\mathrm{II},\mathrm{I}} & \mathbf{K}_{\mathrm{II},\mathrm{II}} \end{pmatrix}, \quad \mathbf{F} = \begin{pmatrix} \mathbf{F}_{\Gamma,\mathrm{I}} & \mathbf{F}_{\Gamma,\mathrm{II}} \\ \mathbf{F}_{\mathrm{I},\mathrm{I}} & \mathbf{F}_{\mathrm{I},\mathrm{II}} \\ \mathbf{F}_{\mathrm{II},\mathrm{I}} & \mathbf{F}_{\mathrm{II},\mathrm{II}} \end{pmatrix}, \quad (34)$$

the scattered modes amplitudes $\mathbf{A}_\mathrm{I}^-$ and $\mathbf{A}_\mathrm{II}^+$ are found after inversion as

$$\begin{pmatrix} \partial_n \mathbf{p}_\mathrm{int} \\ \mathbf{A}_\mathrm{I}^- \\ \mathbf{A}_\mathrm{II}^+ \end{pmatrix} = \mathbf{K}^{-1}\mathbf{F} \begin{pmatrix} \mathbf{A}_\mathrm{I}^+ \\ \mathbf{A}_\mathrm{II}^- \end{pmatrix}. \quad (35)$$

In practice, the summation in (3) is limited to the number of propagative modes as well as some evanescent modes which are included to ensure a precise approximation of the pressure field in the inlet and outlet boundaries. Thus, the scattering matrix system is of a relatively small size. Furthermore, integrals arising in (32) are analytically resolved and there is no need for approximate Gaussian integration. Before we end this section, it may be noted that (35) merely reduces to standard mode matching scattering systems when no cavities are present. In this respect, the Green's function formalism in the lined duct offers the great advantage in that it yields a reduced S-matrix connecting directly the two rigid portions of the duct without the need for expanding explicitly the acoustic pressure in the lined duct mode basis.

5. Results and validations

5.1. Helmholtz resonator on a rigid wall duct

The first example concerns the effect of one Helmholtz resonator connected to a rigid wall duct of height $h = 0.043$ m. This example is inspired by a previous study [5] and shown in Figure 3a. For the sake of illustration, Figure 4 shows typical eigenmode patterns for three resonators with different neck extensions (in order of appearance: straight, with conical contraction and with conical expansion). Dimensions have been chosen to be very similar to its 3D version given in [5].

We are interested in the Transmission Loss (TL) is defined as the ratio of transmitted acoustic power with respect to the incident one. For an incident plane wave, we have

$$\mathrm{TL} = -10 \log_{10} \left(\frac{1}{\beta_0^0 \left| A_{\mathrm{I},0}^+ \right|^2} \sum_{m \geq 0} \beta_m^0 \left| A_{\mathrm{II},m}^+ \right|^2 \right), \quad (36)$$

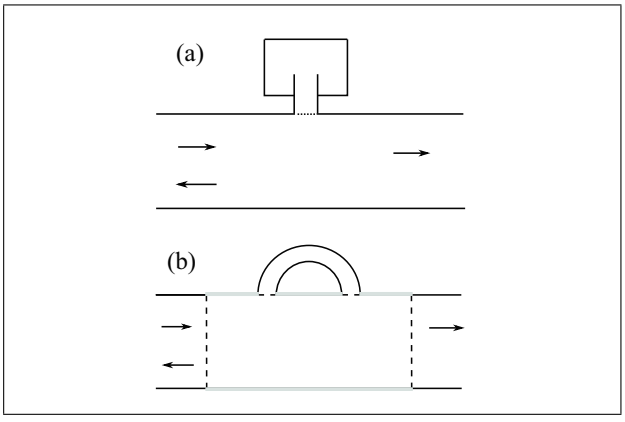

Figure 3. Typical acoustic components.(a): Helmholtz resonator connected to a rigid-wall duct. (b): HQ tube connected to a lined section of a duct (gray color).

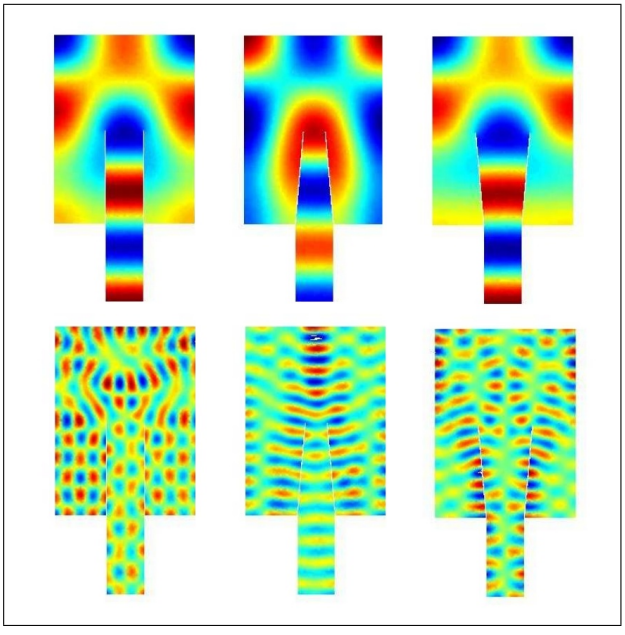

Figure 4. Eigenmodes in the Helmholtz resonators.
Top: Mode #13 (around 2800 Hz) and Bottom: Mode #215 (around 15400 Hz).

where the summation is limited to propagative modes only. In order to validate the method, a full FE model is used. Radiation conditions at both ends of the duct have been implemented using the DtN map [14] using the rigid mode basis expansion. In Figure 5 are plotted the TL calculated from our method (S-matrix) and the FE model showing a very good agreement.

The number of FE nodes is very large compared to number of variables used in our model, i.e. the number of nodes at the interface + the number of modes in the summation in (3), which does not exceed 30, this is reported in Table I. At higher frequency, this number is expected to grow very mildly with the frequency whereas the FE model would quickly become intractable because of the computational overhead. The modal basis in the resonator is computed with about 5000 FE nodes and the first 250 modes are kept

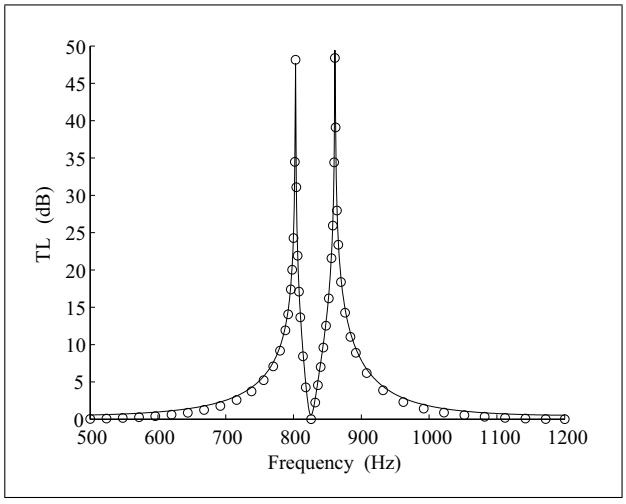

Figure 5. Transmission Loss curve for the Helmholtz resonator with straight extended neck: full FE model (solid line), S-matrix (symbols).

Table I. Comparison of the proposed method (S-matrix) with a full FE model for the Helmholtz resonator. (*) time corresponding to 500 TL calculations on a single PC 2.93 GHz using MATLAB.

	CPU time(*)	FE mesh	Total dof
S-matrix	3 s	5000	< 30
full FE model	8 min	12000	12000

in the calculation. This operation is performed in about 5s using appropriate sparse eigenmode solvers from MATLAB. As the main duct is rigid, there is no need to find the lined duct Green's function and coupling coefficients are diagonal, i.e. $C_{mn} = \delta_{m,n}$; this explains the very low CPU time. Note, in all calculations, the modal series for the duct Green's function is truncated by keeping the first 250 terms in the series to ensure that the diagonal dominant coefficients of the interface-interface interaction matrix $\mathbf{K}_{\Gamma,\Gamma}$ are computed with sufficient accuracy. Figure 6 shows the Transmission Loss for the three Helmholtz resonators. In particular, the shape of the extended necks has a noticeable effect on resonance and anti-resonance frequencies.

5.2. HQ tube on lined wall duct

The second example concerns the effect of a HQ tube placed in the lined section of the duct (see Figure 3). The width of the main duct is $h = 0.04859$ m and the length of the liner is 0.6 m. The study is carried out from very low frequency up to 5000 Hz with a stepsize of 10 Hz. In the overall frequency range, the incident pressure is a plane wave. The first cut-off frequency occurs at $kh = \pi$ which corresponds to 3523 Hz. For the lined wall, the impedance value are chosen as to be in line with perforate plates encountered in the aeronautic industry. Thus, we take $Z_1 = Z_0(2 + 2\mathrm{i})$ and $Z_2 = Z_0(1 + 1\mathrm{i})$ where $Z_0 = \rho c$ denotes the characteristic impedance. Note that

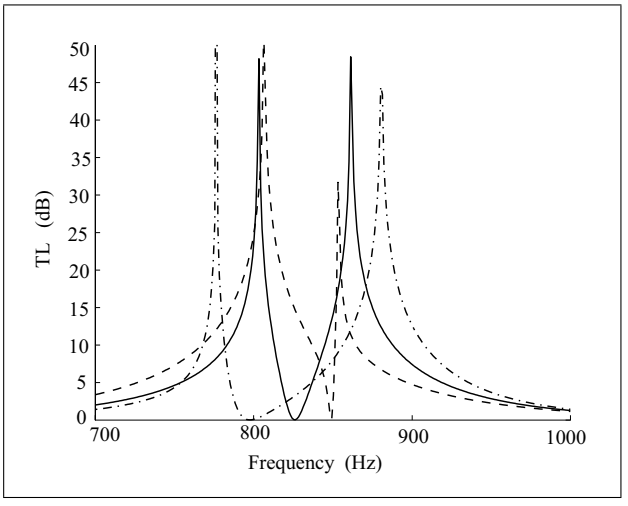

Figure 6. Influence of the extended neck on the Transmission Loss: straight (solid line), conical expansion (dot-dashed line), conical contraction (dashed line).

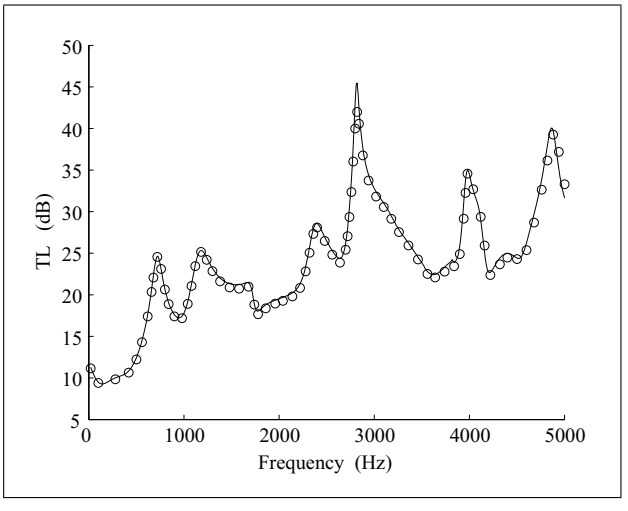

Figure 7. Transmission Loss curve for a HQ tube connected to a lined duct: full FE model (solid line), S-matrix (symbols).

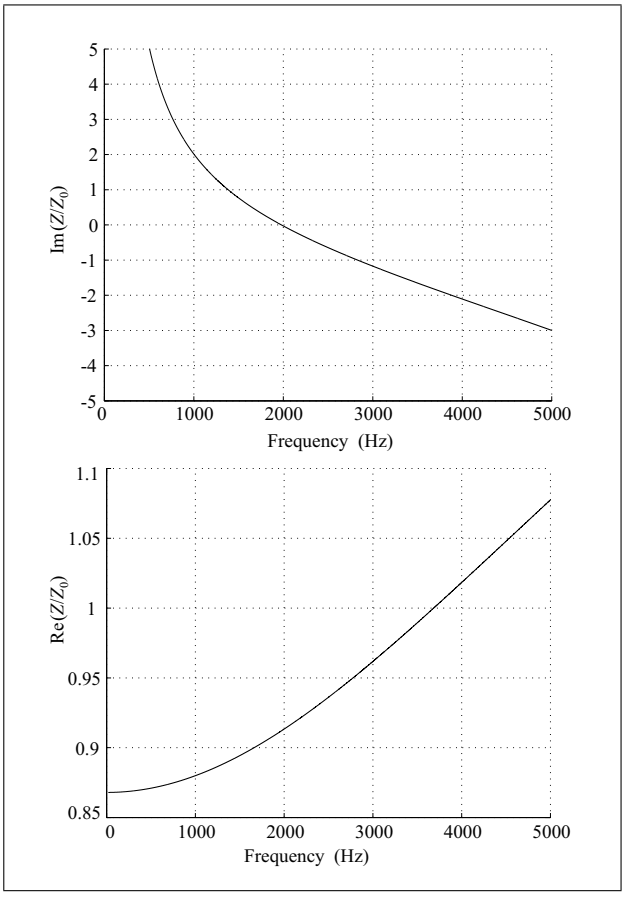

Figure 8. Impedance of the perforate plate (from [2]).

Table II. Comparison of the proposed method (S-matrix) with a full FE model for the HQ tube. (*) time corresponding to 500 TL calculations on a single PC 2.93 GHz using MATLAB.

	CPU time(*)	FE mesh	Total dof
S-matrix	35 s	2500	< 50
full FE model	8 min	11500	11500

the expected frequency dependence of the impedance is not taken into account here but this can be easily included in the analysis as shown in the next example. The HQ tube is about 27 cm long with a width of 4.6 cm and the first 250 modes are included for the impedance matrix (the FE mesh contains about 2500 elements).

In Figure 7 are plotted the Transmission Loss with respect to frequency calculated with both methods. Again, results are in very good agreement and the small discrepancies noticeable at high frequency are thought to be due to the FE model which starts loosing accuracy. The gain in terms of CPU time and memory requirement is shown in Table II. In our calculation, lowest-order modes up to $n = 10$ are pre-computed in the overall frequency range using the NR root finding algorithm whereas other modes are calculated using the asymptotic expansion (with $K = 5$). The size of the S-matrix comprises the number of FE nodes on both interfaces of the HQ tube (approximately 20 nodes) and the number of propagative and evanescent modes in the rigid portion of the duct. In this study, it was found that taking 10 to 15 modes each side was more than sufficient. When the duct is rigid, the problem is simplified since evanescent modes do not need to be included in the calculation.

In the next example, we shall investigate the benefit of the HQ concept for noise control purposes. Though the analysis is carried out in a two dimensional domain, it is believed that some of the results might be relevant for more realistic (3D) configurations. Here, the same duct is considered, except the impedance of the liner is now frequency dependent. The values of the surface impedance are taken form a perforate model [2] and are plotted in Figure 8. The maximum of absorption is expected around 2000 Hz (the imaginary part of the impedance is nearly zero). In this study, three HQ tubes of various shapes and dimensions are tested, this is shown in Figure 9). For an incident plane wave, the Transmission Loss has been computed in the overall frequency range and this is reported in

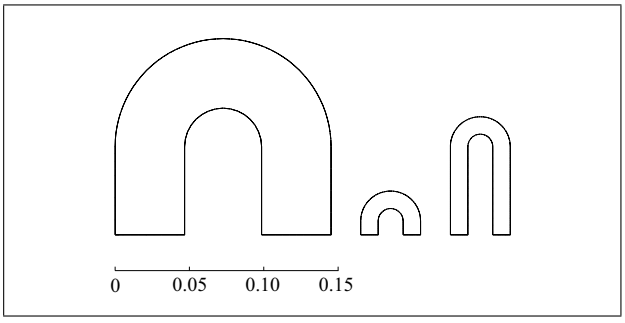

Figure 9. HQ tubes shapes. From left to right: HQ tube #1, HQ tube #2, HQ tube #3. (Dimensions are given in meters).

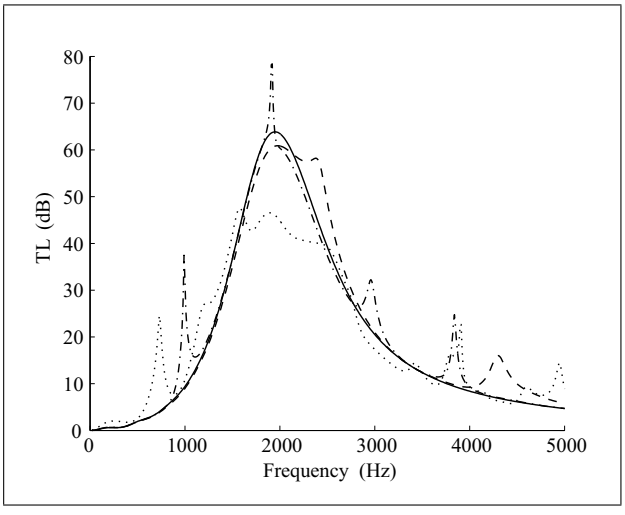

Figure 10. Transmission Loss of lined duct for different configurations: no tube (solid line), HQ tube #1(dotted line), HQ tube #2 (dashed line), HQ tube #3 (dot-dashed line).

Figure 10. In all cases, the HQ tube is positioned 10cms from the inlet plane. Clearly, the best performances are obtained using HQ tube #3. The broadband attenuation offered by the liner is not diminished due to the presence of the tube whereas tonal attenuation located approximately around 1000 Hz, 2000 Hz, 3000 Hz and 3800 Hz are clearly visible. Once the 'best' tube has been identified, it is easy to investigate the effect of its position. Since the modal basis of the tube is already calculated, the remeshing step that would be necessary using a full FE model is not needed here. The only modification in the S-matrix is the translation along z of the nodes and FE elements of the interface. The study has been carried out for various positions (this takes no more than few minutes) but this did not show noticeable effects on the Transmission Loss so results are deliberately not shown in the present paper.

6. Conclusion and prospects

In this paper, a new numerical procedure that judiciously exploit the benefit of the FEM and the BEM approach for the analysis of the sound transmission through lined ducts containing passive components has been presented. Through various examples of practical interest, the method has shown to be extremely beneficial, both in term of CPU time and model reduction, when compared to standard FE models. Work is on going by the present authors to extend the method for more realistic 3D configurations. The presence of an absorbent material in the cavity will also be considered for future work. Finally, we think that the method could be extended for the analysis of other noise reduction techniques such as dissipative silencers that contain porous material for instance. It is hoped that this could have a significant impact in design optimization of flow duct systems.

Aknowledgements

The authors would like to acknowledge the financial support of the CNRS and SNECMA, as well as insightful discussions with SNECMA.

References

[1] J. S. Alonso, R. A. Burdisso, H. W. Kwan, S. Byrne, E. Chien: Experimental investigation of the HQ-liner concept on a scale simulated turbofan rig. 11th AIAA/CEAS Aeroacoustics Conference, U.S., 2005.

[2] B. Poirier, C. Maury, J.-M. Ville: The use of Herschel-Quincke tubes to improve the efficiency of lined ducts. Applied Acoustics **72** (2011) 78–88.

[3] Computational acoustics of noise propagation in fluids. – In: Finite and Boundary Element Methods. S. Marburg, B. Nolte (eds.). Springer, 2008.

[4] K. Gerdes, F. Ihlenburg: On the pollution effect in FE solutions of the 3D-Helmholtz equation. Comput. Methods Appl. Mech. Engrg. **170** (1999) 155–172.

[5] A. Selamet, I. Lee: Helmholtz resonator with extended neck. J. Acoust. Soc. Am. **113** (2003) 1975–1985.

[6] T. W. Wu, P. Zhang, C. Y. R. Cheng: Boundary element analysis of mufflers with an improved method for deriving the four-pole parameters. J. Sound Vib. **217** (1998) 767–779.

[7] P. Juhl: Non-axisymmetric acoustic propagation in and radiation from lined ducts in a subsonic uniform mean flow: An axisymmetric boundary element formulation. Acta Acustica united with Acustica **86** (2000) 860–869.

[8] A. Selamet, N. S. Dickey: The Herschel-Quincke tube: A theoretical, computational, and experimental investigation. J. Acoust. Soc. Am. **96** (1994) 3177–3185.

[9] P. M. Morse, K. U. Ingard: Theoretical acoustics. Princeton University Press, 1968.

[10] R. D. Ciskowski, C. A. Brebbia (eds.): Boundary element methods in acoustics. Computational Mechanics Publications, 1991.

[11] E. Redon, A.-S. Bonnet-Ben Dhia, J.-F. Mercier, S. Poernomo Sari: Non-reflecting boundary conditions for acoustic propagation in ducts with marechalacoustic marechaltreatment and mean flow. Int. J. Numer. Meth. Engng (2011) DOI: 10.1002/nme.3108.

[12] P. Kravanja, M. Van Barel: Computing the zeros of analytic functions. Springer, 2000.

[13] B. Nennig, E. Perrey-Debain, M. B. Tahar: A mode matching method for modelling dissipative silencers lined with poroelastic materials and containing mean flow. J. Acoust. Soc. Am. **128** (2010) 3308–3320.

[14] I. Harari, I. Patlashenko, D. Givoli: Dirichlet-to-Neumann maps for unbounded wave guides. J. Comput. Phys. **143** (1998) 200–223.